Interference effect between superparamagnetic and spin glass correlated moments in a system of dispersed $Co_3O_4$ nanocrystallites



2009 J. Phys.: Condens. Matter 21 095303

(http://iopscience.iop.org/0953-8984/21/9/095303)

J. Phys.: Condens. Matter **21** (2009) 095303 (11pp) doi:10.1088/0953-8984/21/9/095303

# Interference effect between superparamagnetic and spin glass correlated moments in a system of dispersed $Co_3O_4$ nanocrystallites

**D Branković[1], V Jokanović[1], B Babić-Stojić[1,5], Z Jagličić[2], D Lisjak[3] and D Kojić[4]**

[1] Vinča Institute of Nuclear Sciences, PO Box 522, 11001 Belgrade, Serbia
[2] Institute of Mathematics, Physics and Mechanics, Jadranska 19, 1000 Ljubljana, Slovenia
[3] Jožef Stefan Institute, Jamova 39, 1000 Ljubljana, Slovenia
[4] Faculty of Mechanical Engineering, Kraljice Marije 16, 11120 Belgrade, Serbia

E-mail: babic@vin.bg.ac.yu

Received 10 July 2008, in final form 16 December 2008
Published 9 February 2009
Online at stacks.iop.org/JPhysCM/21/095303

**Abstract**

An inhomogeneous system of aggregates of $Co_3O_4$ nanocrystallites dispersed in an amorphous $SiO_2$ matrix has been studied. X-ray diffraction and atomic force microscopy reveal a bimodal distribution of crystallite sizes, smaller nanocrystallites with dimension below 10 nm and larger nanocrystallites of about 20 nm. The $Co_3O_4$ nanocrystallites enter the composition of nanograins with dimension 20–60 nm. The nanograins build aggregates with dimension 200–500 nm. A large value of the effective magnetic moment per $Co^{2+}$ ion obtained from the high-temperature susceptibility measurements indicates possible disturbance of the normal spinel structure in which a fraction of $Co^{3+}$ ions also possesses magnetic moment. An analysis based on the temperature dependence of the coercive field has shown that the smaller nanocrystallites behave as superparamagnetic particles with a blocking temperature of about 10 K. Simultaneous existence of two relaxation processes is observed in the frequency dependence of the imaginary part of the ac magnetic susceptibility in the vicinity of $T = 15.8$ K. The temperature dependence of the width of the distribution function of relaxation times obtained from the Cole–Cole diagrams exhibits behaviour characteristic for spin glass dynamics in a temperature range above 17.6 K and is temperature independent below 15.8 K, which is a property of superparamagnetic particles. The variation of the width of the distribution function between 17.6 and 15.8 K indicates that interference of the superparamagnetic and spin glass dynamics occurs. It has been found that average relaxation time increases with decreasing temperature from $\tau_c < 10^{-4}$ s at 17.6 K to $1.5 \times 10^{-1}$ s at 15 K. The increase of the average relaxation time with decreasing temperature, the observed blocking temperature of the superparamagnetic moments at about 10 K and interference appearing between the two spin dynamics suggest that the magnetic moments in the smaller as well as in the larger nanocrystallites are subject to a thermally activated blocking process at low temperatures.

(Some figures in this article are in colour only in the electronic version)

[5] Author to whom any correspondence should be addressed.

 

## 1. Introduction

Magnetic nanoparticles have received much attention because of a variety of their physical properties and the possibility of numerous applications such as in high density magnetic recording media [1], in biomedical applications [2, 3], and as biomagnetic sensors [4]. The effect of nanoparticle structure and interparticle interactions on the behaviour of magnetic nanocomposites is being intensively studied. In a recent work strongly interacting iron nanocrystals embedded in $SiO_2$ were found to exhibit an ultrafast magnetic response to a transient magnetic field [5]. The properties of this iron nanocomposite appear to be very favourable for applications such as ultrafast magnetic sensors. Ultrafast magnetization dynamics of individual nickel nanomagnets has been recorded [6]. The observed large increase in the precession frequency by reduction of magnet diameter is significant for high speed operation of high density magnetic storage devices. Picosecond magnetization dynamics of an array of $Ni_{88}Fe_{12}/Co_{80}Fe_{20}$ bilayer nanoelements were also studied [7]. It was shown that the measured precession was subject to a crossover from the high to low frequency regime as the element size was reduced and that the two observed modes were associated with the edge and centre regions of the nanoelements. It was found that the magnetization dynamics became less uniform as the size of the element was reduced, which could significantly contribute to noise in the read sensors of computer hard disc drives. These results can also be applied to the ultrafast precessional switching of magnetic data storage elements induced by a pulsed magnetic field. A thorough understanding of the material properties, particularly dynamics properties, is essential for utilization of nanomagnets in any application.

In the present work the system of aggregates of $Co_3O_4$ nanocrystallites has been studied. $Co_3O_4$ nanoparticles have attracted considerable interest because of a variety of magnetic properties observed in this system: superparamagnetism, spin glass and magnetic short range order. $Co_3O_4$ bulk crystal is antiferromagnetic with a Néel temperature of 30 K [8–10]. Several studies have been reported recently for the $Co_3O_4$ nanoparticles with uniform size distribution. The particles with crystallite size of about 17 nm exhibited antiferromagnetic ordering of spins with a Néel temperature of 26 K [10]. A narrow cusp in zero-field-cooled (ZFC) magnetization at about 25 K was observed in the $Co_3O_4$ nanoparticles with dimension of 20 nm [11]. The ZFC and field-cooled (FC) magnetization in that work strongly bifurcated at low temperatures, with a rapid increase of the FC magnetization with decreasing temperature. In the system of $Co_3O_4$ nanocrystals with dimension of about 16 nm dispersed in an amorphous silicate, the existence of a spin glass phase was established for higher concentration of Co in the precursor solution [9]. The ZFC magnetization of the very small $Co_3O_4$ nanoparticles with diameters 2–3 nm exhibited a narrow cusp at temperatures between 7.5 and 12 K with a strong bifurcation of the FC and ZFC branches below the characteristic temperature [12, 13]. Such behaviour was attributed to the uncompensated surface spins with superparamagnetic properties just above the blocking temperature and ferromagnetic properties with a small hysteresis below this temperature.

In this work the system with a bimodal distribution of the $Co_3O_4$ nanoparticles dispersed in an amorphous $SiO_2$ matrix has been produced by a sol–gel method. The activated dynamics of the sample is investigated using the phenomenological description of Cole and Cole [14–16]. Simultaneous existence of relaxation phenomena is observed.

The Cole–Cole formalism introduces a parameter $\alpha$ ($0 < \alpha < 1$), which determines the width of distribution of relaxation times, $g(\ln\tau)$, around the average relaxation time $\tau_c$,

$$g(\ln\tau) = \frac{1}{2\pi}\frac{\sin(\alpha\pi)}{\cosh\left[(1-\alpha)\ln(\tau/\tau_c)\right] - \cos(\alpha\pi)}. \quad (1)$$

This distribution is determined from the Cole–Cole equation for the complex magnetic susceptibility [15, 16],

$$\chi = \chi_s + \frac{\chi_0 - \chi_s}{1 + (i\omega\tau_c)^{1-\alpha}}, \quad (2)$$

where $\chi_0$ and $\chi_s$ are the isothermal ($\omega \to 0$) and adiabatic ($\omega \to \infty$) susceptibility respectively. On the basis of the Cole–Cole equation one can determine an expression for the dependence of the imaginary part $\chi''$ on the real part $\chi'$ of the complex magnetic susceptibility, which allows a fit of the experimental data. Such fits with $\alpha$, $\tau_c$, $\chi_0$ and $\chi_s$ as parameters are presented in the Cole–Cole diagrams, where the phenomenological Cole–Cole model is described by circular arcs of size $(1-\alpha)\pi$ cutting the $\chi'$ axis at $\chi_0$ and $\chi_s$ with a maximum at $\omega\tau_c = 1$. The present study enables us to better understand the connection between magnetic properties and nanostructure of the system of dispersed $Co_3O_4$ nanoparticles.

## 2. Experimental details

A $Co_3O_4$–$SiO_2$ powder sample ($w(Co_3O_4) = 0.57$) was obtained by sol–gel processing. The sol was prepared by dissolving $Co(NO_3)_2{\cdot}6H_2O$ in distilled water as 3.88 M solution, and adding 5.96 M $SiO_2$ sol and drops of $NH_4OH$, maintaining the stirring for 30 min. $NH_4OH$ with concentration of 2 M was dropped into the solution until the pH was stabilized during the process. The used molar proportions were chosen to form the composite $(CoO)_{0.5}{\cdot}(SiO_2)_{0.5}$. Gelation of the sol occurred during drying at 150 °C for about 3 days. The gel was ground and annealed at 550 °C for 5 h in air atmosphere.

The sample was initially characterized by infrared (IR) spectroscopy on a Perkin-Elmer 983G spectrophotometer. KBr pellets were used for IR spectra recording. X-ray characterization of the sample was carried out on an Bruker D4 Endeavor automated powder diffractometer using Cu K$\alpha$ radiation. The x-ray diffraction (XRD) pattern was taken in the 10°–110° $2\theta$ range with a step of 0.026° and with exposure time of 20 s/step. Atomic force microscopy (AFM) was carried out in AC-tapping mode using a JSPM-5200 JEOL instrument. Scanning electron microscopy (SEM) was performed using a JSM-6460LV JEOL microscope. Energy

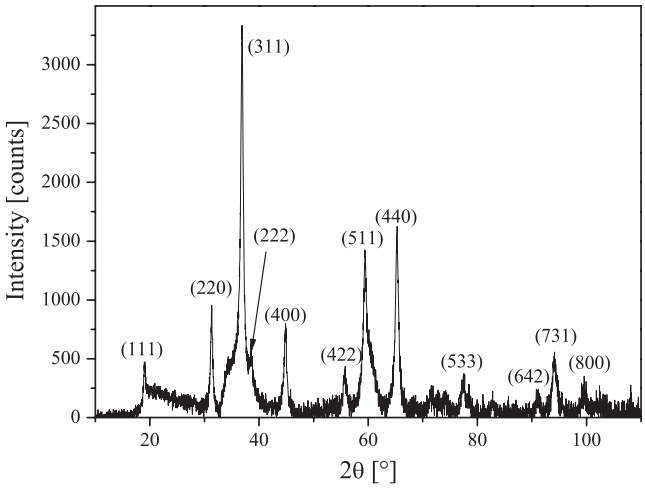


**Figure 1.** X-ray diffraction pattern of the $Co_3O_4$ nanocrystallites dispersed in an amorphous $SiO_2$ matrix.

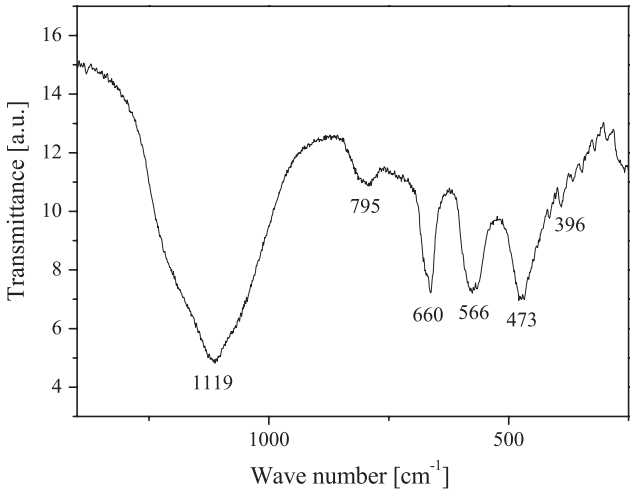


**Figure 2.** Infra-red spectrum of the $Co_3O_4$ nanocrystallites dispersed in an amorphous $SiO_2$ matrix.

dispersive spectroscopy (EDS) associated with SEM was performed using an Oxford INCA Penta Fetx 3 instrument. Magnetic measurements were carried out on a SQUID magnetometer (MPMS-XL-5, Quantum Design) equipped with an ac option. Zero-field-cooled (ZFC) and field-cooled (FC) measurements of the magnetic susceptibility were performed at applied magnetic fields from 8 to 10 000 Oe. The ac magnetization measurements were made using different frequencies in the range 1–1500 Hz under an ac exciting field with amplitude of 6.5 Oe.

## 3. Results and discussion

The XRD pattern of the sample indicates the formation of the spinel phase of $Co_3O_4$. In spite of the high amount of silica in the sample, there is no evidence of crystalline silica, so the $SiO_2$ contained in the sample is amorphous. The XRD pattern of the $Co_3O_4$ nanocrystallites with the background from the silica matrix subtracted is presented in figure 1. On the basis of the expression for interspacing distance $d_{hkl}$ for the cubic crystal lattice it is confirmed that $Co_3O_4$ appears in the space group $Fd\bar{3}m$ ($a = 8.085$ Å). The XRD spectrum of the sample suggests in fact a bimodal distribution of crystallite sizes, larger crystallites (sharp peaks) plus smaller crystallites (broadened peak part just above the background). Using the Pawley method for the crystal size determination [17] the best fit is obtained for the combination of 20 nm plus 2 nm crystallites.

In the IR transmission spectrum measured from 1400 to 250 cm$^{-1}$, the bands due to vibrations of $Co_3O_4$ molecules and of amorphous $SiO_2$ appear (figure 2). These bands are in agreement with the literature data [18–20]. The bands at 660 and 566 cm$^{-1}$ are related to the vibrations of the sublattice of the octahedral groups. Their frequency is essentially determined by the nature of the trivalent cations. The band at 396 cm$^{-1}$ corresponds to complex vibrations relating to the cations either in tetrahedral or octahedral sites. The bands arising from amorphous $SiO_2$ are visible in the IR spectrum at 1119, 795 and 473 cm$^{-1}$.

The particle size and morphology were characterized by atomic force microscopy and scanning electron microscopy. Figures 3(a) and (b) represent AFM images of the $Co_3O_4$ nanocrystalline sample. Smaller nanocrystallites with dimension 5–6 nm can be seen in figure 3(a) along the chosen direction, which is denoted by an arrow. The presence of larger nanocrystallites with dimension about 20 nm can be seen in figure 3(b) along the chosen direction, which is also denoted by an arrow. The existence and dimensions of the smaller and larger nanocrystallites seen by AFM are consistent with the results obtained from the XRD spectrum. Figures 3(a) and (b) reveal that the smaller and larger nanocrystallites enter the composition of nanograins with dimension in the range 20–60 nm. The nanograins are linked together in such a way that they form net-like nanosurfaces having thickness between 20 and 60 nm, which corresponds to the dimension of the nanograins. A scanning electron microscopy image of the net-like nanosurfaces is presented in figure 4(a). The net-like nanosurfaces enter the structure of aggregates with dimension 200–500 nm. The aggregates are cross-linked in rose-like structures with dimension of the order of 1 $\mu$m, which are shown in figure 4(b). One aggregate in the form of a whitish spot denoted by an arrow in figure 4(b) is magnified and shown in figure 4(c). The aggregates of the nanograins can be also seen in figure 4(d). The chemical composition of an aggregate of the nanograins analysed by EDS is presented in figure 5.

In the high-temperature region ($T > 60$ K) the magnetic susceptibility of the sample obeys the Curie–Weiss law with the molar Curie constant $C = 5.5$ emu K mol$^{-1}$ Oe$^{-1}$ and with the Curie–Weiss temperature $\theta = -4$ K, indicating antiferromagnetic interactions between the Co ions, figure 6.

The bulk $Co_3O_4$ exhibits a normal spinel structure with a formula unit $AB_2O_4$, where A and B denote ions in tetrahedral and octahedral sites respectively. In the normal spinel structure only $Co^{2+}$ ions in the tetrahedral sites possess magnetic moment. $Co^{3+}$ ions in the octahedral sites have no permanent magnetic moment due to large crystal field splitting of the 3d orbitals by the octahedral crystal field. On the assumption that

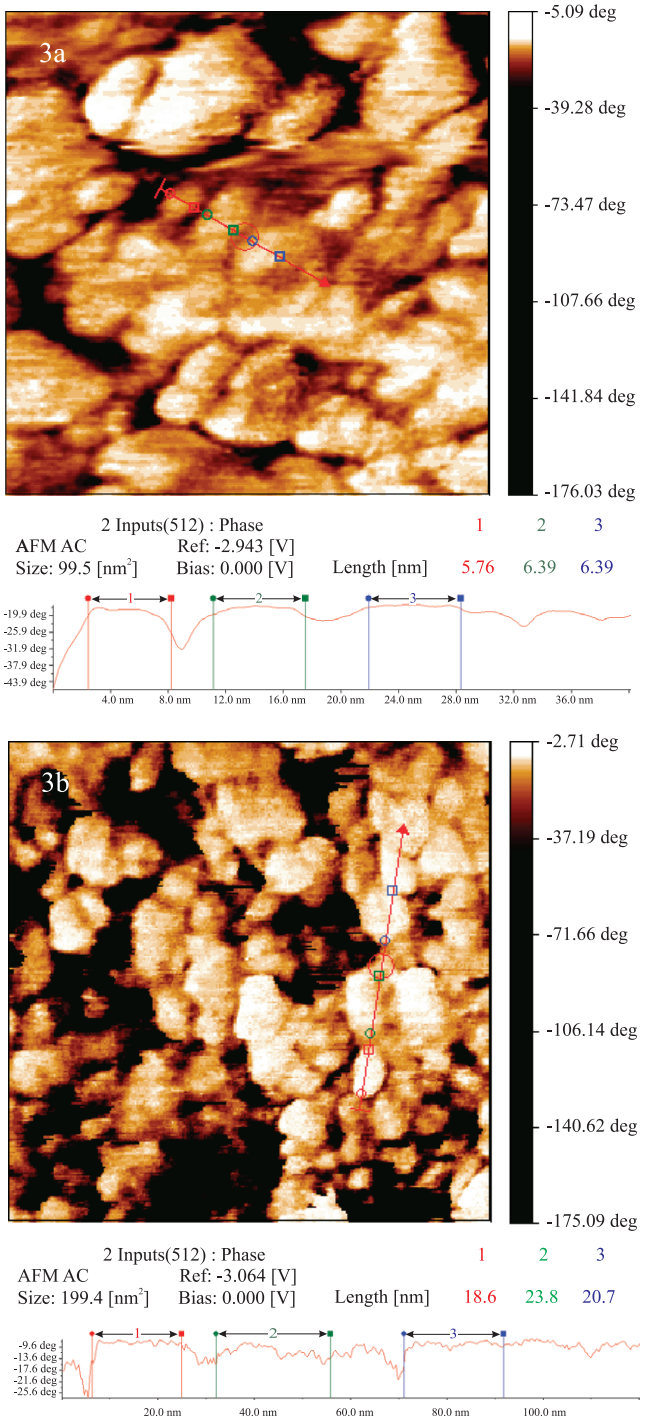


**Figure 3.** AFM images of the $Co_3O_4$ nanocrystallites: (a) smaller nanocrystallites observed along the chosen direction denoted by the arrow, (b) larger nanocrystallites observed along the chosen direction also denoted by the arrow. Both images reveal that the smaller and larger nanocrystallites enter the composition of nanograins.

the $Co_3O_4$ nanocrystals in our sample also have the normal spinel structure, the effective magnetic moment per $Co^{2+}$ ion estimated from $C = N\mu_{\rm eff}^2/3k_{\rm B}$, where $N$ is the number of $Co^{2+}$ ions per mole of $Co_3O_4$, is found to be $\mu_{\rm eff} = 6.65\ \mu_{\rm B}$. The large effective magnetic moment per $Co^{2+}$ ion, compared to the expected value of 4.2 $\mu_{\rm B}$ for the ion with spin $S = 3/2$ and with Landé factor $g = 2.18$ [10], could not be explained assuming that the magnetic moments are localized only on the $Co^{2+}$ ions. It seems that a fraction of the $Co^{3+}$ ions in the nanocrystallites also possesses magnetic moment, which can happen if a part of the $Co^{3+}$ ions is located in the tetrahedral sites of the $Co_3O_4$ spinel structure.

The first derivative of the product $\chi T$ with respect to temperature, $\partial(\chi T)/\partial T$, for the magnetic susceptibility measured at 1000 Oe is presented in the insets of figure 6. It can be seen that there is no peak in the $\partial(\chi T)/\partial T$ versus $T$ plot in the temperature range 25–30 K where the Néel temperature could be expected. Only some small and irregular temperature variations are detected in the region 22–24 K (right inset in figure 6), which are absent from the temperature dependence of $\partial(\chi T)/\partial T$ measured at lower field values, 50 and 100 Oe. In a paper published recently, a Néel temperature of $T_{\rm N} = 30$ K for the bulk and $T_{\rm N} = 26$ K for the $Co_3O_4$ nanoparticles with average crystallite size of 17 nm were recorded from the peaks in the $\partial(\chi T)\partial T$ versus $T$ plot of the magnetic susceptibility data [10]. According to that study, the effective magnetic moment per $Co^{2+}$ ion was found to be 4.27 $\mu_{\rm B}$ for the bulk and 4.09 $\mu_{\rm B}$ for the $Co_3O_4$ nanoparticles, which correspond to the normal spinel structure. In the study of the antiferromagnetic order in the polycrystalline $Co_3O_4$ sample, a sharp peak at 29 K of the function $\partial(\chi T)/\partial T$ versus $T$ was observed, and the effective magnetic moment per $Co^{2+}$ ion estimated from the high-temperature susceptibility was obtained as 4.79 $\mu_{\rm B}$ [21]. It should be noted that at a temperature of about 12 K a small dip in the temperature dependence of $\partial(\chi T)/\partial T$ for our sample is recorded (left inset in figure 6). Although this dip is very small, it is also detected at the same temperature in the applied magnetic fields of 50, 100 and 10 000 Oe.

The temperature dependence of magnetic susceptibility measured in zero-field-cooled and field-cooled conditions is shown in figure 7. The ZFC and FC susceptibilities of our nanocrystalline sample clearly bifurcate at low temperatures. The temperature at which the ZFC and FC curves start to bifurcate lies between 17 and 11 K for the applied magnetic field from 8 to 10 000 Oe respectively. Below the bifurcation temperature and for lower values of the magnetic field the ZFC susceptibility abruptly decreases, whereas the FC susceptibility exhibits flattening at temperatures $T < 10$ K.

The magnetic field dependence of magnetization at several temperatures is presented in figure 8. It can be seen that the $M(H)$ dependence at 50 K is a linear function in the magnetic field range up to 50 kOe showing paramagnetic origin of the magnetization at higher temperatures. At low temperatures (2 and 5 K) a hysteresis loop is clearly observed. There is no saturation in magnetization even at the highest applied field of 50 kOe. The $M(H)$ dependence at low temperatures is also characterized by relatively large coercive fields (the inset in figure 8).

Figure 9 shows the variation of the coercive field with temperature. We find that at low temperatures the coercive field obeys the relation

$$H_{\rm c}(T) = H_{\rm c0}\left[1 - \left(\frac{T}{T_{\rm B}}\right)^{1/2}\right], \qquad (3)$$

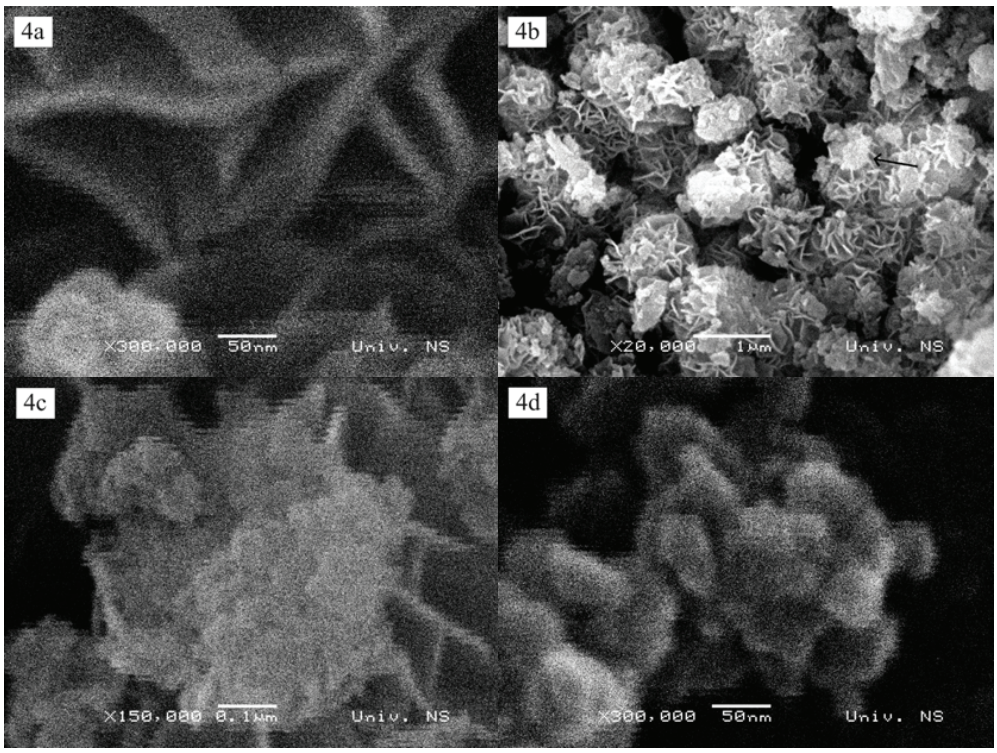


**Figure 4.** SEM micrographs of the $Co_3O_4$ nanocrystalline sample: (a) net-like nanosurfaces with thickness 20–60 nm; (b) aggregates of nanograins cross-linked in the rose-like structures; the arrow in this image shows an aggregate in the form of a whitish spot; (c) magnified detail from micrograph (b); (d) more detailed image of the aggregates of nanograins.

where $H_{c0}$ is the zero temperature coercivity and $T_B$ is the blocking temperature of the magnetic particles [22–24]. The extrapolation of $H_c(T)$ to zero field yields for our sample the value of $T_B = 9.9$ K.

The inverse value of relaxation time of a particle magnetic moment is proportional to the probability $\exp(-KV/k_BT)$ that a particle has enough thermal energy to overcome the energy barrier $\Delta E = KV$, where $K$ is the magnetic anisotropy constant and $V$ is the particle volume. Below the blocking temperature $T_B$ thermal activation is not sufficient to allow the immediate alignment of the particle moments with the applied magnetic field. For the relaxation time $\tau$ approximately equal to the measurement time of a hysteresis loop (about 1 h), we can write $T_B = K\langle V\rangle/30\ k_B$, where $\langle V\rangle$ is the average particle volume and the number 30 is obtained from $\ln(\tau f_0)$ with frequency factor $f_0 = 10^9$ s$^{-1}$ [22]. Using the value of the magnetic anisotropy constant for the $Co_3O_4$ nanocrystals $K = 9 \times 10^5$ erg cm$^{-3}$ [25], and the blocking temperature obtained from the $H_c(T)$ dependence, the average particle volume is calculated as $\langle V\rangle = 4.6 \times 10^{-20}$ cm$^3$. For spherical particles the volume $\langle V\rangle$ corresponds to the average particle diameter $\langle D\rangle = 4.4$ nm. This value is in good agreement with the dimension of the smaller nanocrystallites, 5–6 nm, observed in the AFM image. This result suggests that the smaller nanocrystallites in the sample with particle size less than 10 nm behave as superparamagnetic particles, whose magnetic moments are blocked against the thermal fluctuation energy below the blocking temperature $T_B$. In the studies of the $Co_3O_4$ nanocrystals and other materials in the nanocrystalline form with particle size below 10 nm reported so far superparamagnetic properties of the particles have been observed: a hysteresis loop with low coercive fields below the blocking temperature $T_B$ [12, 23–26]; scaling of the $M(H)$ dependence against $H/T$ for $T > T_B$ [23, 24, 26]; Langevin type dependence of the magnetization versus magnetic field at temperatures $T > T_B$ [23–26]. However, in our sample large coercive fields of the order of 1 kOe at low temperatures (2 and 5 K) are observed.

Magnetic field reduces the energy barrier of the nanoparticles [22]. If the nanoparticles are subject to the influence of the magnetic field of non-superparamagnetic entities, or to the influence of the coercive field of non-superparamagnetic entities, then it could lead to a dependence of this field (coercive field) on temperature which is described by equation (3). A fit of the Langevin function to the measured magnetization versus magnetic field at $T = 20$ K, which lies above $T_B$, does not give a satisfactory result. The possible reasons for this disagreement could be the existence of interparticle interactions, inhomogeneous particle size distribution, nanocrystalline magnetic anisotropy, antiferromagnetic contribution to the magnetization and paramagnetic state of the magnetic moments at higher temperatures. The observed flattening of the FC magnetic susceptibility curves at temperatures below 10 K (figure 7) seems to arise from interactions among the nanoparticles.

Figure 10 shows the temperature dependence of (a) the real part $\chi'$ and (b) the imaginary part $\chi''$ of the ac magnetic susceptibility at different frequencies. It can be seen that

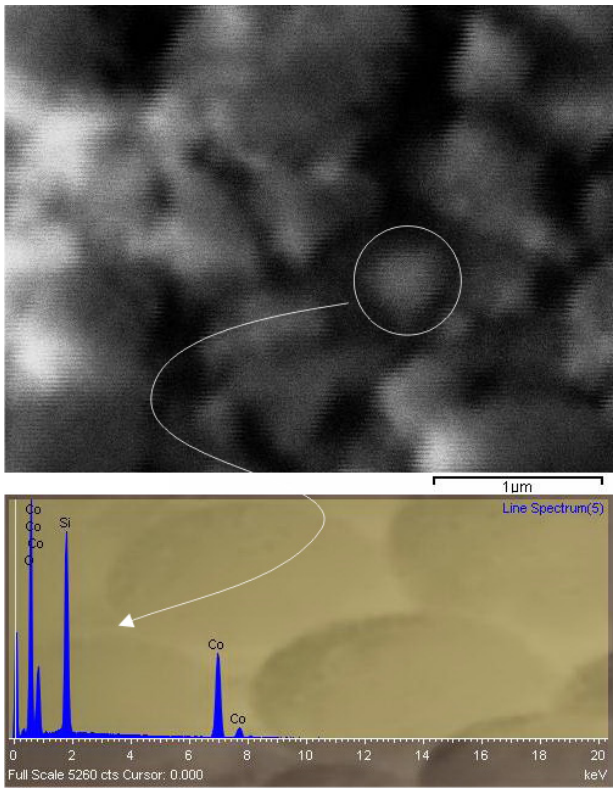


**Figure 5.** SEM micrograph of the $Co_3O_4$ nanocrystalline sample. The chemical composition of an aggregate of nanograins is shown in the form of an EDS spectrum in the lower part of the figure.

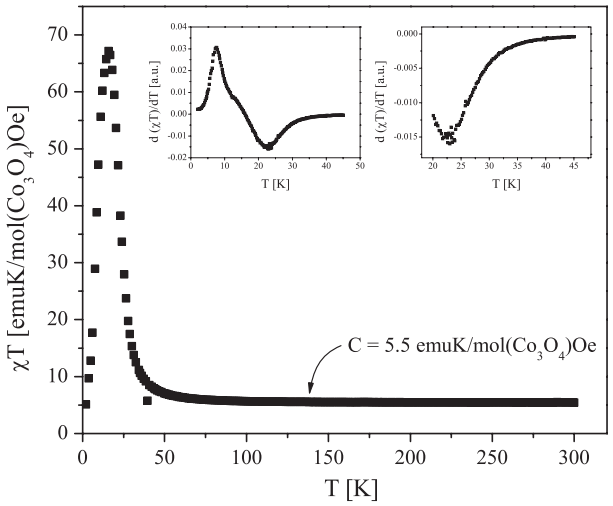


**Figure 6.** Temperature dependence of the product $\chi T$ measured at the magnetic field of 1000 Oe. Insets: first derivative of the product $\partial(\chi T)/\partial T$ versus temperature in the two temperature regions.

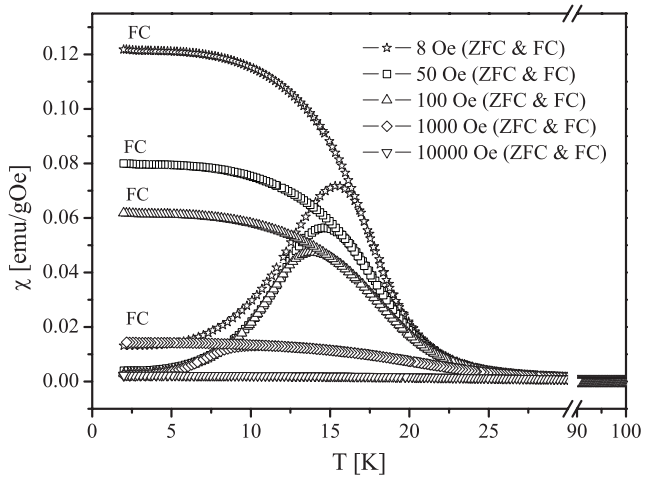


**Figure 7.** Temperature dependence of the magnetic susceptibility under the zero-field-cooled (ZFC) and field-cooled (FC) conditions at different magnetic fields in the range 8–10 000 Oe.

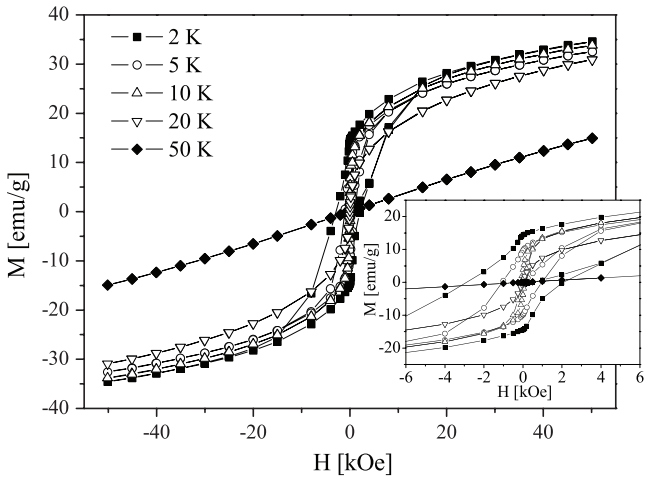


**Figure 8.** Magnetic field dependent magnetization at several selected temperatures. The inset shows the $M(H)$ dependence in the lower field region.

the real component $\chi'$ has a maximum at a temperature $T_f$, which shifts towards higher temperatures with increasing frequency. This property is characteristic of most of the spin glass systems [15, 27–30], but also of the interacting and noninteracting superparamagnetic nanoparticles [25, 31]. On the other hand, the imaginary part $\chi''$ versus temperature curves detected at various frequencies are almost zero at higher temperatures, $T > 20$ K, and are appreciably enhanced around and below $T_f$.

In the analysis of the frequency dependence of the temperature $T_f$ we have firstly attempted to fit the data to the Arrhenius law, which is usually used for noninteracting superparamagnetic particles, $f = f_0 \exp(-E_a/k_B T_f)$, where $E_a$ is the energy required for reversal of magnetic moment orientation and $f_0$ is the frequency factor. However, this fit gives completely unphysical values, $f_0 = 2 \times 10^{38}$ Hz and $E_a/k_B = 1336$ K. If one fits the frequency dependent temperature of the maximum in the imaginary component of the ac magnetic susceptibility to the Arrhenius law, similar unphysical values for $f_0$ and $E_a$ are obtained. A quantitative measure of the frequency shift of the temperature $T_f$ is obtained from the ratio $\Delta T_f/[T_f \Delta \log f]$. From the set of the $\chi'$ versus temperature curves measured at different frequencies presented in figure 10 we have estimated $\Delta T_f/[T_f \Delta \log f] = 0.02$. This quantity varies in the range 0.005–0.01 for the canonical

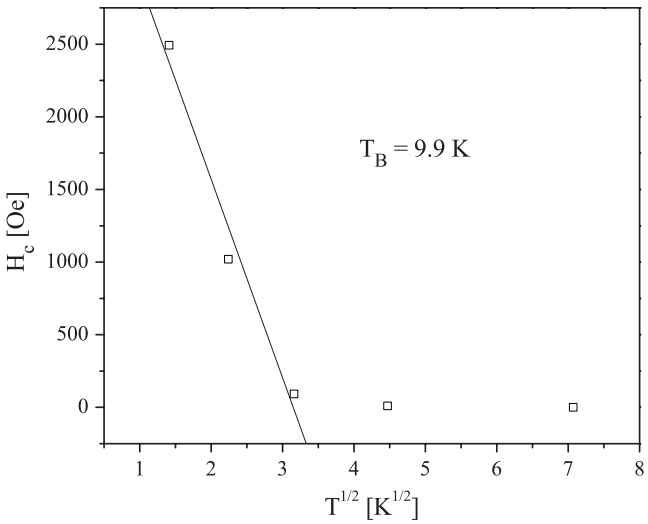


**Figure 9.** Temperature dependence of the coercive field. The solid line represents the fit of the dependence (equation (3)) to the experimental data.

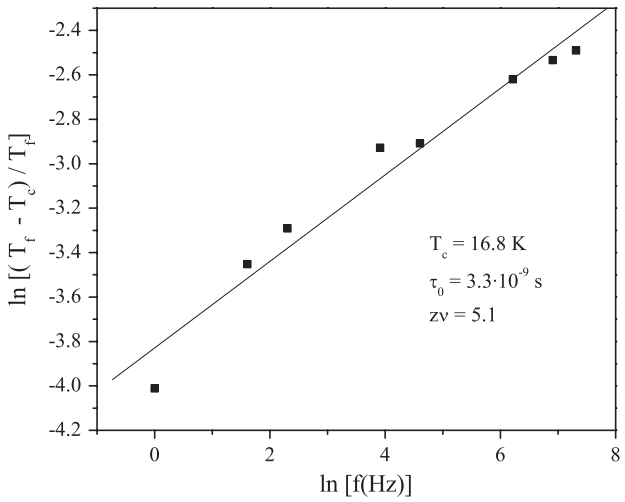


**Figure 11.** Fit of the power law dependence (equation (4)) describing the frequency dependent freezing temperature $T_f$ to the experimental data.

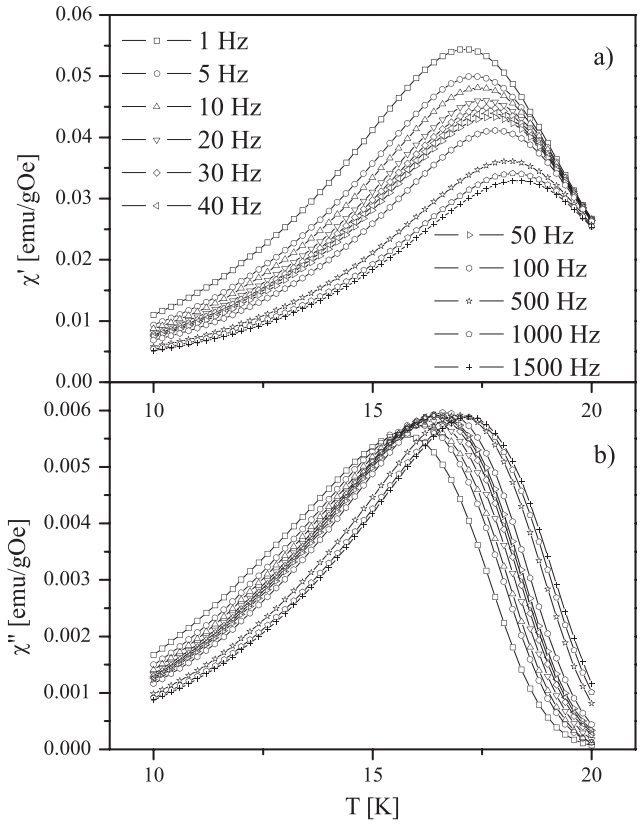


**Figure 10.** Temperature dependence of the (a) real ($\chi'$) and (b) imaginary ($\chi''$) parts of the ac magnetic susceptibility at different frequencies in the range 1–1500 Hz.

spin glasses, from 0.01 to 0.08 for various semiconducting and insulating spin glasses, and is of the order of 0.3 for some superparamagnets [29]. It appears that the shift of the temperature $T_f$ per decade of frequency for our sample is consistent with the values for typical semiconducting and insulating spin glass materials.

The frequency dependent data have been also examined by conventional critical slowing down [29],

$$\tau = \tau_0 \left[ \frac{T_f}{T_f - T_c} \right]^{z\nu}, \qquad (4)$$

where $T_f$ is the frequency dependent freezing temperature at which the maximum relaxation time $\tau$ of the system corresponds to the measured frequency, $\tau_0$ is a microscopic relaxation time, $T_c$ should correspond to the dc equilibrium value of $T_f(f \rightarrow 0)$ and the product $z\nu$ is the dynamical exponent. A good fit of the power law dependence (4) to the experimental data is obtained for $\tau_0 = 3.3 \times 10^{-9}$ s, $T_c = 16.8$ K and $z\nu = 5.1$ (figure 11). In the canonical spin glass CuMn (4.6 at.%) $z\nu = 5.5$, $\tau_0 = 10^{-12}$ s, and in the various semiconducting and insulating spin glasses $z\nu$ is in the range 4–12 and $\tau_0$ varies in the range $10^{-7}$–$10^{-13}$ s [32–35]. The frequency dependent temperature $T_f$ for our sample satisfies the power law dependence (4) with the parameters $\tau_0$ and $z\nu$ which are consistent with the values obtained for other conventional spin glasses. The shift of the temperature $T_f$ per decade of frequency, estimated from the quantity $\Delta T_f/[T_f \Delta \log f]$, also agrees with the values for typical semiconducting and insulating spin glass materials. These experimental findings indicate that the observed maximum in the ac magnetic susceptibility (figure 10) arises from the spin glass freezing of the magnetic moments in the sample.

As pointed out, the smaller $Co_3O_4$ nanocrystallites with particle size below 10 nm behave as superparamagnetic particles. A small dip recorded in the temperature dependence of $\partial(\chi T)/\partial T$ at about 12 K (left inset in figure 6) could be an indication of a Néel temperature of the smaller nanocrystallites. In a paper published recently [31] a Néel temperature of about 15 K for the $Co_3O_4$ nanoparticles with average diameter of 4 nm has been observed. It appears that the variation of $T_N$ is a function of the nanoparticle size [36], and for the particles with average diameter below 10 nm it can be considerably lower than that in the bulk.

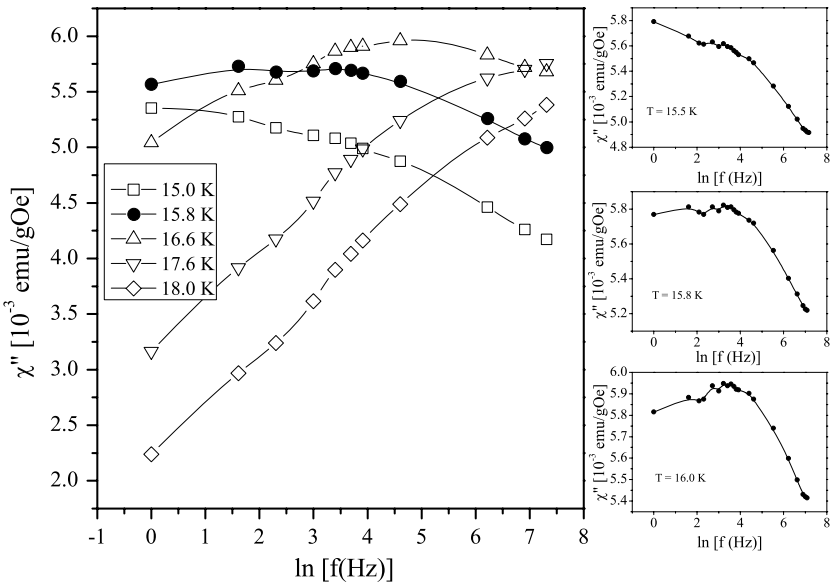


**Figure 12.** Imaginary part $\chi''$ of the ac magnetic susceptibility as a function of frequency at several selected temperatures. Two maxima in the $\chi''$ component versus logarithm of frequency observed at temperatures 15.8 and 16.0 K are shown in the central and lower insets of the figure. The curves are guides to the eye.

However, no peak in the temperature dependence of the dc magnetic susceptibility, nor in the temperature dependence of $\partial(\chi T)/\partial T$ at $T > 25$ K, which could be associated with the Néel temperature of the larger nanocrystallites, has been detected. This result, as well as the fact that we observe magnetic properties of the sample which are characteristic for the spin glass dynamics, suggest an assumption that a fraction of the $Co^{2+}$ and $Co^{3+}$ ions in the larger nanocrystallites could be randomly distributed over the tetrahedral and octahedral sites of the $Co_3O_4$ spinel structure. The large value of the effective magnetic moment per $Co^{2+}$ ion obtained from the high-temperature susceptibility data under the assumption of the normal spinel structure has already indicated that a fraction of the $Co^{3+}$ ions is probably located in the tetrahedral sites of the spinel structure. The presumed random distribution of the $Co^{2+}$ and $Co^{3+}$ ions could be the origin of the spin glass behaviour of the sample, which is observed as the maximum in the ac magnetic susceptibility near 17 K (figure 10) and as the bifurcation of the ZFC and FC curves in the dc magnetic susceptibility between 17 and 11 K depending on the applied magnetic field (figure 7). It is interesting to note that in the $Co_3O_4$ nanocrystals with particle size of about 17 nm and with preserved normal spinel structure, antiferromagnetic ordering of the $Co^{2+}$ ion spins in the core of the nanocrystals below $T_N$ was detected [10]. In the case of a disturbance of the normal spinel structure, where a fraction of the $Co^{3+}$ ions also possesses magnetic moment, there is an alteration of the magnetic properties of the system. It appears that the alteration of the magnetic properties of our sample manifests itself in the spin glass relaxation of the Co ion magnetic moments. The absence of saturation in the $M(H)$ dependence and large coercive fields detected in the sample at low temperatures (figure 8) are in accordance with those observed in other spin glass systems [34, 35].

A more complete description of the experimental data than that following from the phenomenological laws is obtained from the Cole–Cole analysis of the ac magnetic susceptibility in the frequency range 1–1500 Hz and over the temperature range where the relaxation phenomena are observed (figure 10). The frequency dependence of the imaginary part of the ac magnetic susceptibility at several temperatures from 15 to 18 K is shown in figure 12. A maximum in this dependence at higher frequency can be seen at temperature $T = 17.6$ K when the presence of the low frequency maximum is hardly observable. The maximum at lower frequency is developed with decreasing temperature at the expense of the maximum at higher frequency. At temperature $T = 15.8$ K two maxima in the dependence of $\chi''$ on logarithm of frequency is observed (central inset in figure 12). Two maxima in the dependence of $\chi''$ on $\ln f$ can be also recognized at temperature $T = 16.0$ K at nearly the same frequencies as those recorded at 15.8 K (lower inset in figure 12). These two maxima reveal the simultaneous existence of two relaxation processes.

In order to get better insight into the relaxation time distribution, the susceptibility data are plotted in the complex plane $\chi''$ versus $\chi'$, where each frequency represents a point. These diagrams (the Cole–Cole diagrams) [15] for different temperatures around the spin glass freezing temperature $T_f$ are presented in figure 13. In the case of a single relaxation time $\tau$, these diagrams would consist of half circles with maxima in $\chi''$ where $\omega\tau = 1$. For our sample $\chi''$ versus $\chi'$ diagrams deviate from the half circles with arc length $(1 - \alpha)\pi$, which gives an estimation of the width of the distribution function of relaxation times, equation (1). The most important characteristic of the spin relaxation in our system is that the two relaxation processes occur in the temperature range investigated which can be seen in the Cole–Cole diagram for $T = 15.8$ K (the inset in figure 13).

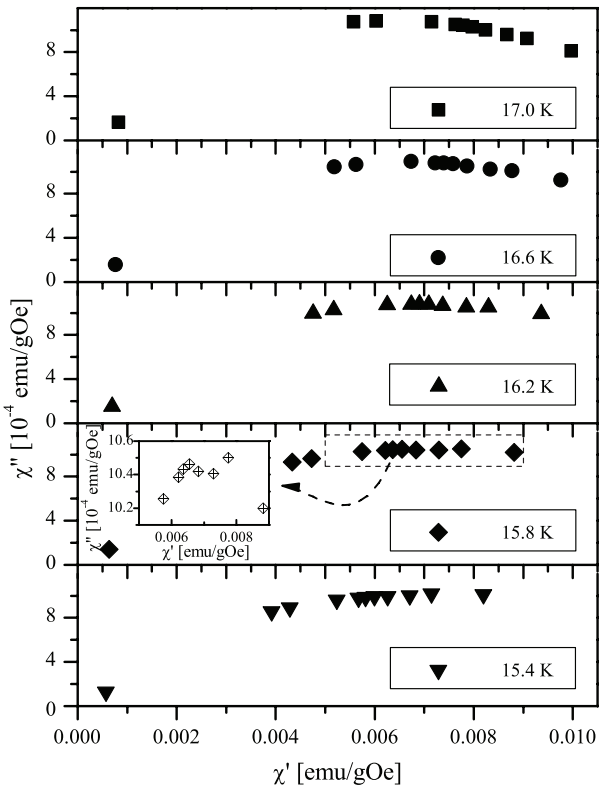


**Figure 13.** Cole–Cole diagrams for several selected temperatures. Each point in the Cole–Cole diagrams refers to one of the frequencies in the range 1–1500 Hz.

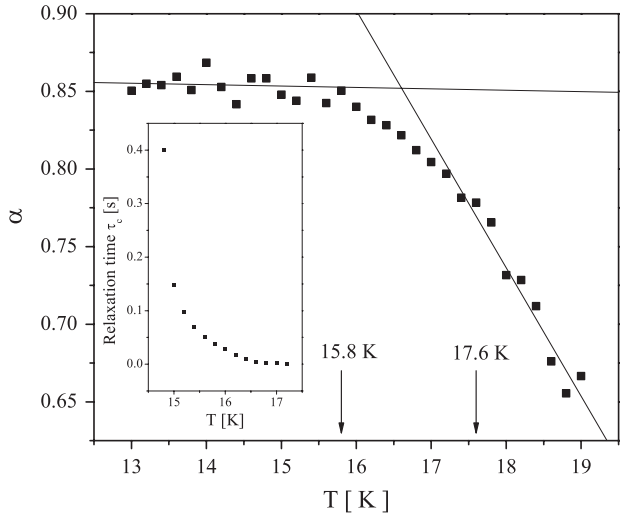


**Figure 14.** Temperature dependence of the parameter $\alpha$ representing the width of the distribution function of relaxation times derived from the Cole–Cole analysis. Inset: temperature dependence of the average relaxation times $\tau_c$ derived from the Cole–Cole analysis.

The width of the distribution function of relaxation times $\alpha$ determined from the Cole–Cole diagrams is presented as a function of temperature in figure 14. It can be seen that the parameter $\alpha$ has approximately a linear temperature dependence in the temperature range from about 17.6 K up to the highest temperature at which the Cole–Cole analysis has been performed. This dependence is typical for the spin glass dynamics and was found in several spin glass systems [15, 16]. At temperatures below 15.8 K the parameter $\alpha$ is temperature independent with a value of about 0.85 (figure 14). The temperature independent width of the distribution function is typical for the superparamagnetic particles [16]. Variation of the parameter $\alpha$ at temperatures from 17.6 to 15.8 K indicates that an interference of the spin glass dynamics and dynamics characteristic for superparamagnetic relaxation occurs. At temperatures $T = 15.8$ and 16.0 K the simultaneous existence of two relaxation processes is clearly seen in the frequency dependent imaginary component of the ac magnetic susceptibility (figure 12). Structural, magnetic and size dependent properties of the $Co_3O_4$ nanocrystals in the investigated sample indicate that the superparamagnetic behaviour and relaxation could arise from the smaller nanocrystallites with particle size below 10 nm, whereas the spin glass properties probably originate in the larger nanocrystallites with dimension of about 20 nm. Interference appearing between the two spin dynamics indicates significant magnetic interaction between the two magnetic entities.

The simultaneous existence of two relaxation processes observed in the frequency dependent imaginary component of the ac magnetic susceptibility (figure 12) manifests itself as one maximum in the temperature dependence of the imaginary component of the ac magnetic susceptibility (figure 10(b)). In several previously published papers [37, 38], two types of clusters in the spinel structure $Co_{0.2}Zn_{0.8}Fe_{1.95}Ho_{0.05}O_4$ were examined, small clusters containing $Fe^{3+}$ ions which exhibited spin glass freezing at lower temperature and large clusters with $Fe^{3+}$ and $Ho^{3+}$ ions showing superparamagnetic blocking at higher temperature. In that system two independent maxima in the imaginary part of the ac susceptibility versus temperature, belonging to two spin dynamics, were observed. In our sample superparamagnetic relaxation of the smaller nanocrystallites and spin glass dynamics attributed to the larger nanocrystallites are mutually dependent, leading to a superposition to one maximum in the temperature dependence of the absorption part of the ac magnetic susceptibility.

The average relaxation time $\tau_c$, obtained from the Cole–Cole diagrams so that each diagram is approximated by a circular arc having one maximum at $\omega\tau_c = 1$, is presented in the inset of figure 14. The very limited range of temperatures in which the average relaxation time is determined (from 14.8 to 17.2 K) is dependent on the relatively narrow range of frequencies (1–1500 Hz) which we could apply in the ac magnetization measurements. An estimation of the average relaxation time at temperature $T = 17.6$ K gives $\tau_c < 10^{-4}$ s. With decreasing temperature the average relaxation time increases. As can be seen in the inset of figure 14, there is no jump or even divergence in the temperature dependence of $\tau_c$ in the vicinity of $T = 17$ K, as one might expect on the basis of the critical slowing down of the spin relaxation time described by equation (4). Smooth variation of $\tau_c$ near 17 K could be due to interference of the superparamagnetic and spin glass dynamics developed in the smaller and larger $Co_3O_4$ nanocrystallites which are aggregated inside the nanograins. Significant increase of the average relaxation time at a temperature just below 15 K is

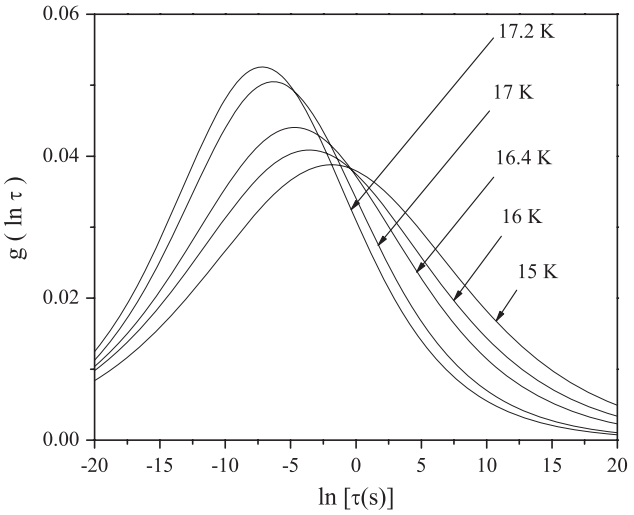


**Figure 15.** Distribution of relaxation times $g(\ln \tau)$ for several selected temperatures derived from the Cole–Cole analysis.

detected. With further temperature decrease, a large increase of $\tau_c$ is expected as the temperature approaches $T = 10$ K, which has been recognized as the blocking temperature of the superparamagnetic nanoparticles in the system.

The parameters $\alpha$ and $\tau_c$ determined from the Cole–Cole analysis at each temperature allow the construction of the distribution function of relaxation times, figure 15. In the temperature range where it was possible to determine the average relaxation time, this distribution covers seven decades at $T = 17.2$ K and ten decades in width (full width at half maximum) at $T = 15$ K. In the same time the distribution shifts as a whole towards larger times as the temperature decreases. The maximum of the distribution function is at $\tau_c = 0.8 \times 10^{-3}$ s for $T = 17.2$ K and $\tau_c = 1.5 \times 10^{-1}$ s for $T = 15$ K. The tmperature dependent part of the width of the distribution function arises from spin glass correlated magnetic moments (spin glass clusters) whose correlation length and corresponding relaxation times increase with decreasing temperature. According to the temperature dependence of the parameter $\alpha$, below $T = 15.8$ K the influence of dynamics of the superparamagnetic moments is stronger, leading to a temperature independent width of the distribution of relaxation times. The increase of the average relaxation time $\tau_c$ with decreasing temperature, the observed blocking temperature of the superparamagnetic moments at about 10 K and interference appearing between the two spin dynamics suggest that the magnetic moments in the smaller as well as in the larger nanocrystallites are subject to a thermally activated blocking process at low temperatures.

## 4. Conclusion

Structural and magnetic properties of the inhomogeneous system of $Co_3O_4$ nanocrystallites dispersed in an amorphous $SiO_2$ matrix have been studied. The $Co_3O_4$ nanocrystallites have a bimodal distribution of crystallite sizes, the smaller nanocrystals with dimension below 10 nm and larger nanocrystals of about 20 nm. An analysis based on the temperature dependence of coercive field has shown that the smaller nanocrystallites behave as superparamagnetic particles. The frequency dependence of the temperature of the maximum in the real part of the ac magnetic susceptibility is found to be in agreement with that observed in other conventional spin glasses. A large value of the average magnetic moment per $Co^{2+}$ ion, obtained from the high-temperature susceptibility data on the assumption that the magnetic moments are localized only on the $Co^{2+}$ ions, indicates possible disturbance of the normal spinel structure in which a fraction of the $Co^{3+}$ ions also possesses magnetic moment. Simultaneous existence of two relaxation processes in our sample is observed in the frequency dependence of the imaginary part of the ac magnetic susceptibility in the vicinity of $T = 15.8$ K. The temperature dependence of the width of the distribution of relaxation times exhibits behaviour characteristic for the spin glass dynamics in a temperature range above 17.6 K, and is temperature independent below 15.8 K, which is a property of superparamagnetic particles. The variation of the width of the distribution of relaxation times at temperatures from 17.6 to 15.8 K indicates that an interference between superparamagnetic and spin glass dynamics occurs. Average relaxation time (averaged over the both relaxation processes) is found to increase with decreasing temperature. The increase of the average relaxation time with decreasing temperature, the observed blocking temperature of the superparamagnetic moments at about 10 K and interference appearing between the two spin dynamics suggest that the magnetic moments in the smaller as well as in the larger nanocrystallites are frozen at low temperatures.

## Acknowledgments

Financial support for this study was granted by the Ministry of Science of the Republic of Serbia, project Nos 141013 and 142066. We are grateful to Miloš Bokorov for producing the SEM images and Zoran Nedić for the IR measurements. We also thank Branko Matović for useful discussion and Dušan Milivojević for technical assistance.

## References

[1] Terris B D and Thomson T 2005 *J. Phys. D: Appl. Phys.* **38** R199
[2] Berry C C and Curtis A S G 2003 *J. Phys. D: Appl. Phys.* **36** R198
[3] Anderson E A, Isaacman S, Peabody D S, Wang E Y, Canary J W and Kirshenbaum K 2006 *Nano Lett.* **6** 1160
[4] Chung S H, Hoffmann A, Bader S D, Liu C, Kay B, Makowski L and Chen L 2004 *Appl. Phys. Lett.* **85** 2971
[5] Buchanan K S, Zhu X, Meldrum A and Freeman M R 2005 *Nano Lett.* **5** 383
[6] Barman A, Wang S, Maas J D, Hawkins A R, Kwon S, Liddle A, Bokor J and Schmidt H 2006 *Nano Lett.* **6** 2939
[7] Kruglyak V V, Barman A, Hicken R J, Childress J R and Katine J A 2005 *Phys. Rev.* B **71** 220409
[8] Roth W L 1964 *J. Phys. Chem. Solids* **25** 1
[9] Sato M, Kohiki S, Hayakawa Y, Sonda Y, Babasaki T, Deguchi H and Mitome M 2000 *J. Appl. Phys.* **88** 2771

[10] Dutta P, Seehra M S, Thota S and Kumar J 2008 *J. Phys.: Condens. Matter* **20** 015218
[11] Makhlouf S A 2002 *J. Magn. Magn. Mater.* **246** 184
[12] Ichiyanagi Y, Kimishima Y and Yamada S 2004 *J. Magn. Magn. Mater.* **272–276** e1245
[13] Ichiyanagi Y and Yamada S 2005 *Polyhedron* **24** 2813
[14] Cole K S and Cole R H 1941 *J. Chem. Phys.* **9** 341
[15] Dekker C, Arts A F M, de Wijn H W, van Duyneveldt A J and Mydosh J A 1989 *Phys. Rev.* B **40** 11243
[16] Hüsser D, van Duyneveldt A J, Nieuwenhuys G J and Mydosh J A 1986 *J. Phys. C: Solid State Phys.* **19** 3697
[17] Pawley G S 1981 *J. Appl. Cryst.* **14** 357 software Topas 2R (Burker AXS, Kalsruhe, Germany)
[18] Preudhomme J and Tarte P 1971 *Spectrochim. Acta* **27** A 1817
[19] Casado P G and Rasines I 1984 *J. Solid State Chem.* **52** 187
[20] Lenglet M and Lefez B 1996 *Solid State Commun.* **98** 689
[21] Ikedo Y, Sugiyama J, Nozaki H, Itahara H, Brewer J H, Ansaldo E J, Morris G D, Andreica D and Amato A 2007 *Phys. Rev.* B **75** 054424
[22] Cullity B D 1972 *Introduction to Magnetic Materials* (Menlo Park, CA: Addison-Wesley)
[23] McHenry M E, Majetich S A, Artman J O, DeGraef M and Staley S W 1994 *Phys. Rev.* B **49** 11358
[24] Fonseca F C, Goya G F, Jardim R F, Muccillo R, Carreno N L V, Longo E and Leite E R 2002 *Phys. Rev.* B **66** 104406
[25] Takada S, Fujii M, Kohiki S, Babasaki T, Deguchi H, Mitome M and Oku M 2001 *Nano Lett.* **1** 379
[26] Dutta P, Manivannan A, Seehra M S, Shah N and Huffman G P 2004 *Phys. Rev.* B **70** 174428
[27] Tholence J L 1980 *Solid State Commun.* **35** 113
[28] Fiorani D, Viticoli S, Dormann J L, Tholence J L and Murani A P 1984 *Phys. Rev.* B **30** 2776
[29] Mydosh J A 1993 *Spin Glasses: an Experimental Introduction* (London: Taylor and Francis)
[30] Koyano M, Suezawa M, Watanabe H and Inoue M 1994 *J. Phys. Soc. Japan* **63** 1114
[31] Resnick D A, Gilmore K, Idzerda Y U, Klem M T, Allen M, Douglas T, Arenholz E and Young M 2006 *J. Appl. Phys.* **99** 08Q501
[32] Karmakar S, Taran S, Chaudhuri B K, Sahata H, Sun C P, Huang C L and Yang H D 2006 *Phys. Rev.* B **74** 104407
[33] Bontemps N, Rajchenbach J, Chamberlin R V and Orbach R 1984 *Phys. Rev.* B **30** 6514
[34] Dho J, Kim W S and Hur N H 2002 *Phys. Rev. Lett.* **89** 027202
[35] Wang F, Zhang J, Chen Y, Wang G, Sun J, Zhang S and Shen B 2004 *Phys. Rev.* B **69** 094424
[36] He L, Chen C, Wang N, Zhou W and Guo L 2007 *J. Appl. Phys.* **102** 103911
[37] Bhowmik R N and Ranganathan R 2002 *J. Magn. Magn. Mater.* **247** 83
[38] Bhowmik R N, Ranganathan R and Nagarajan R 2006 *J. Magn. Magn. Mater.* **299** 327